Special Issue

Applied Spectroscopy

www.s-a-s.org

Confocal Raman Microscopy as a Probe of Material Deconstruction in Processed Low-Density Polyethylene Particles

Applied Spectroscopy
1–10

DOI: 10.1177/00037028251322142
journals.sagepub.com/home/asp
Sage

Md. Wahiduzzaman[1,†], Jeremy Lawrence[1,†], Ashley Moreno-Gongora[1], Jiahe Xu[1], Dominick J. Casadonte[1], Gerardine G. Botte[2] and Carol Korzeniewski[1]

Abstract

Confocal Raman microscopy was applied to detect structural change within individual particles of low-density polyethylene (LDPE) following chemical and electrochemical processing steps that aimed to facilitate material decomposition. A high numerical aperture (NA) oil-immersion objective enabled depth-profiling through the near surface region (20 μm–40 μm) of irregularly shaped particles with an axial spatial resolution < 2 μm estimated from measurements of instrument detection efficiency profiles. Changes in vibrational bands sensitive to polyethylene crystallinity were evident following treatments and linked to the release of low molecular weight compounds present as additives and products of processing. Effects of processing were probed by monitoring the rise of Raman scattering intensity in vibrational modes associated with polyethylene chains in a zig-zag (trans) conformation near 1128 cm^{-1}, 1294 cm^{-1}, and 1418 cm^{-1}, signaling chain clustering and development of organized, crystalline-like assemblies. Pristine LDPE particles displayed a uniform structure across the near surface region, while particles treated initially with chemical extractant and then further processed displayed increasingly enhanced crystallinity up to the maximum depth probed (40 μm). As a step toward measurements on ensembles of particles, least squares modeling was adapted to derive pure component spectra reflecting crystallinity change within spectral datasets. The work demonstrates high spatial resolution Raman depth-profiling for the characterization of processed polymers using a high NA immersion objective to overcome the limitations of air-objectives often used for confocal Raman microscopy.

Keywords

Confocal Raman microscopy, Raman depth-profiling, low-density polyethylene, polymer deconstruction, least squares modeling

Date received: 17 November 2024; accepted: 29 January 2025

Introduction

The explosive growth in the production and use of plastics during the past 70 years has led to deleterious environmental impacts worldwide.[1,2] Furthermore, it has been estimated that less than 10% of these plastics have been recycled, with roughly 80% having found their place in landfills or the natural environment.[1] The accumulation of discarded plastics in soil and waterways is a leading concern today, particularly in relation to natural degradation processes that cause fragmentation and the formation of micro- and nano-scale plastic particles, so-called microplastics (MPs) and nano plastics (NPs), respectively.[3–5] The ease of entry of MPs and NPs into water systems and the atmosphere is a significant concern for human health and safety.[4–7]

To aid the effort to responsibly manage discarded plastics through energy efficient recycling or upcycling, Rahimzadeh and co-workers recently demonstrated an approach based on electrochemical processing that achieved functionalization and deconstruction of low-density polyethylene (LDPE) particles.[8] Carried out at ambient temperature and pressure, the reaction conditions promoted LDPE particle surface oxidation and the formation of low molecular weight chain scission products. Among the material characterization techniques employed, Raman microscopy was explored to follow reaction progress and detect the changes in polymer crystallinity that accompany chain scission.

[1]Department of Chemistry and Biochemistry, Texas Tech University, Lubbock, Texas, USA
[2]Institute for Sustainability and Circular Economy, Department of Chemical Engineering, Whitacre College of Engineering, Texas Tech University, Lubbock, Texas, USA
[†]These authors contributed equally.

Corresponding Author:
Carol Korzeniewski, Department of Chemistry and Biochemistry, Texas Tech University, Lubbock, Texas 79409-1061, USA.
Email: carol.korzeniewski@ttu.edu

Raman microscopy is sensitive to molecular composition within the near surface region of materials.[9] With careful attention to refractive index matching and diffraction-limited focusing, a confocal Raman microscope can attain sub-micrometer spatial resolution measuring within the surface plane of a sample (in-plane) and a few micrometers depth-profiling below the surface (axially).[9–14] Refractive index matching is typically achieved through the use of a water- or oil-immersion objective.[10,12,13,15–17] Compared to air objectives, which are commonly used for Raman microscopy and designed to focus into the sample through an air gap, immersion objectives can operate with a higher numerical aperture (NA) and thereby provide greater light collection efficiency and improved sensitivity.[9–13,15–17] In recent years, Raman experiments performed using high NA immersion objectives have shown the sensitivity and spatial resolution needed to support nanoscale probing of liquid–solid interfaces[15] and for depth-profiling within layered polymer membranes.[10,13,16–19] Also benefiting from tight focusing and high collection efficiency, the strategy has been applied extensively in the Harris lab to measure chemical composition and perform quantitative chemical assays within individual, micrometer-scale particles (see for example Bridges et al.,[20] Kitt et al.,[21] Bryce et al.,[22] Myres et al.[23,24]). With the confocal probe volume positioned centrally within a particle, these latter studies have shown analyte extracted into the host matrix[20] or chemically modified pores[21–24] can be easily detected and quantified down to sub-nanomole levels.[21–23]

The work discussed herein adapts from the strategies mentioned above. A confocal Raman microscope equipped with a high NA oil-immersion objective is used to measure within individual polyethylene particles following processing steps that aim to achieve chemical functionalization or decomposition of the polymer in support of upcycling and recycling efforts. Depth profiles and single point measurements obtained within 50 μm of the particle surface show the effects of processing steps on polymer structure within the near surface region.

Experimental

Materials and Methods

The LDPE powder composed of nominally 500 μm diameter particles was obtained from Thermo Fisher Scientific (USA; Alfa Aesar division, Catalog no. A10239). Hexane extraction and electrochemical processing of LDPE was performed in accordance with procedures in Rahimzadeh et al.[8] Electrolyte solutions were prepared from deionized water dispensed at 18 MΩ·cm resistivity from a Purelab ultra water purification system (Elga LabWater, USA). H_2O_2 (30 wt%) was from Macron Fine Chemicals (USA). *n*-Hexane (high-performance liquid chromatography grade, Lot 61169) was from Supelco Analytical Products (a division of Millipore-Sigma, USA). Carboxylated polystyrene microspheres (10 μm) were from Polysciences (USA), and poly (dimethylsiloxane) (PDMS) was obtained from Thermo Fisher Scientific. Unless noted otherwise, all chemicals were reagent grade or better purity and used as received.

Extraction of LDPE Powder. As described in Rahimzadeh et al.[8] (Scheme S2, Supplemental Material), organic additives were removed from LDPE particles by extraction in *n*-hexane under reflux at 50 °C. LDPE powder (initially 10 g) was suspended in 200 mL of solvent and refluxed for two hours under continuous stirring. The powder was isolated by vacuum filtration and the extraction repeated three times using fresh hexane for each. Particles were dried at 80 °C under vacuum and stored in glass vials prior to analysis using Raman microscopy.

Sonication Processing. Sonication processing was performed using a Sonics and Materials VC 750 direct-immersion sonicator operating at 20 kHz and nominal acoustic power of 0.4 W/cm^3.[25] LDPE particles and polyethylene microspheres were suspended in 3 wt% H_2O_2 (prepared by dilution of stock 30 wt% H_2O_2 in deionized water) and underwent sonication at 23 °C in a jacketed cell for a reaction period of 60 minutes.

Confocal Raman Microscopy. The Raman microscope was home-built and constructed as described earlier.[26] Briefly, a beam from a 660 nm single-mode diode-pumped solid-state laser (Gem 660, 0.75 ± 0.15 mm beam diameter, Laser Quantum, USA) was expanded (7×; Special Optics, USA) and then directed toward the rear entrance port of an Olympus IX73 inverted microscope (Olympus USA). To slightly overfill the rear aperture of the microscope objective (100×, 1.45 NA, Olympus UPLXAPO, 130 μm working distance, 5.2 mm rear aperture), the beam was spectrally filtered (FF01-640/40-25, Semrock, USA) and reflected from a dichroic mirror (DI03-R660-T1-25X36, Semrock). The objective brought the excitation radiation into an individual LDPE particle resting on top of a microscope coverslip (no. 1.5, 0.17 mm thickness, BK-7 glass, 22 mm × 22 mm) through a film of immersion oil. Backscattered Raman light was collected through the same microscope objective. The radiation was focused onto the entrance slit (50 μm) of a grating monochromator (Shamrock 500i, Andor, UK) after passing the dichroic mirror and transmission through a final long-pass filter (LP02-664RU-25, Semrock). The diffraction grating, 300 lines/mm blazed at 760 nm, dispersed Raman scattered light from the slit image onto a charge-coupled device (CCD) camera (iDus DU416A, Andor). The resolution achieved was 1.66 cm^{-1}/pixel. The confocal aperture was defined using the entrance slit of the monochromator in the horizontal dimension and by binning three rows of pixels on the CCD camera (45 μm) in the vertical dimension.[12,13,27,28] This collection aperture, together with the excitation beam focus (approximately 0.6 μm diameter) defines an ideal, diffraction limited confocal probe volume for the system with 90% detection efficiency located within a depth along the axial direction of ±1.2 μm.[12,13] Unless

stated otherwise, the spectral acquisition time was 60 s. Spectral acquisition was under the control of SOLIS software (v.4.32, Andor). The laser was operated at 30 mW.

Spectral measurements were recorded from particles that had been dispersed onto the surface of a glass microscope coverslip (0.17 mm thickness, no. 1.5, BK-7 glass). Particles were observed visually in the eyepiece and moved into the sampling position using *x*,*y* (in-plane) stage controls. The Alfa Aesar particles were irregular in shape and care was taken to perform measurements at points where the polymer contacted the glass to ensure reasonable refractive index matching across the sample/glass interface.[9,10,12] A glass microscope slide could be placed over dispersed particles to improve stability and polymer/glass contacts, and a droplet of water could be added to enhance throughput. Additionally, light easily coupled into polyethylene spheres that were adherent to the coverslip after depositing spheres from a suspension in water and drying in air until the particle settled on the microscope coverslip. Following in-plane positioning, the confocal probe volume was raised within a particle to the desired depth.

Data Processing. Spectral data processing was performed on desktop computers using custom scripts executed in Matlab (v.R2022a; The MathWorks, Inc., USA). After subtraction of a dark current offset, Raman spectra were corrected for instrument response by ratioing to a recorded spectrum of emission from a standard reference halogen source lamp (SL1-CAL, StellarNet, USA).[29–31] Spectral baselines were corrected using a rolling-circle[32] high-pass filter. Scripts for PCA (factor analysis)[33,34] and least squares regression analysis[35–37] utilized the Matlab pca and fminsearch functions, respectively. Significance testing[33] of PCA loadings was performed during *pca* function execution using Matlab's built-in Hotelling's T-squared statistic. To compensate for differences in probe volume characteristics among samples, where comparisons are made spectral intensities are reported as relative to the intensity of the strong anti-symmetric CH_2 stretching vibrational mode for polyethylene near 2882 cm^{-1} (Figure 1).

Results and Discussion

Spectral Measurements on Individual Particles

Figure 1 shows a Raman spectrum recorded from a polyethylene particle in contact with the surface of a glass microscope coverslip. The bands that appear in Figure 1 are characteristic of LDPE.[38,39] The strong peaks at 2849 cm^{-1} and 2882 cm^{-1} arise from symmetric and anti-symmetric CH_2 stretching vibrations, respectively.[39,40] The bands at lower frequency have been studied recently in connection with polyethylene crystallinity and structural ordering.[38,39,41,42] These lower frequency bands have been applied to monitor structural change in response to photo-[39–41] and bio-degredation[39–42] processing. The features at 1061 cm^{-1}, 1128 cm^{-1}, and 1294 cm^{-1} arise from vibrations of polyethylene chains in a zig-zag (trans) conformation.[41,42] The intensities of the latter two bands, assigned to symmetric C–C stretching and CH_2 twisting motions, respectively, display strong sensitivity to crystallinity and grow as trans chains cluster and form organized assemblies.[38,39,41,42] The complex feature near 1440 cm^{-1} is associated with CH_2 bending and deformation motions[38,41,42] and is affected by Fermi resonance[40] interactions. The sharp peak toward the low energy side near 1418 cm^{-1} is a signature of the orthorhombic crystalline phase.[40–42] Full band assignments are summarized in Table I.

Figure 2 expands the low frequency region of Raman spectra collected from polyethylene particles prior to and following various processing steps. In all cases, the confocal probe volume sampled ~20 μm from the particle surface. Since these LDPE particles were somewhat irregular in shape,

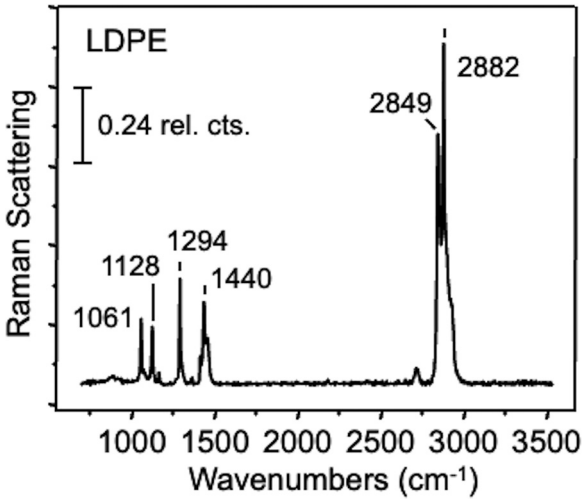

Figure 1. Raman spectrum recorded from an individual, nominally 500 μm diameter particle of pristine LDPE in contact with the surface of a glass microscope coverslip. The confocal probe volume was located at a depth of approximately 20 μm from the particle surface. Spectral intensities are relative to the 2882 cm^{-1} peak.

Table I. LDPE Raman band assignments.[38,40,41]

Band (cm^{-1})	Assignment[a]
1061	ν_{as}(C–C) (trans)
1080	ν(C–C) (amorphous)
1128	ν_s(C–C) (trans)
1298	$\tau(CH_2)$ (trans)
1305	$\tau(CH_2)$ (amorphous)
1415	$\delta(CH_2) + \omega CH_2$ (crystalline)
1440	$\delta(CH_2)$ (amorphous)
1460	$\delta(CH_2)$ (amorphous)
2849	ν_s(C–H)
2882	ν_{as}(C–H)

[a]ν_s: symmetric stretching; ν_{as}: asymmetric stretching; ν: stretching; τ: twisting; δ: bending; ω: wagging.

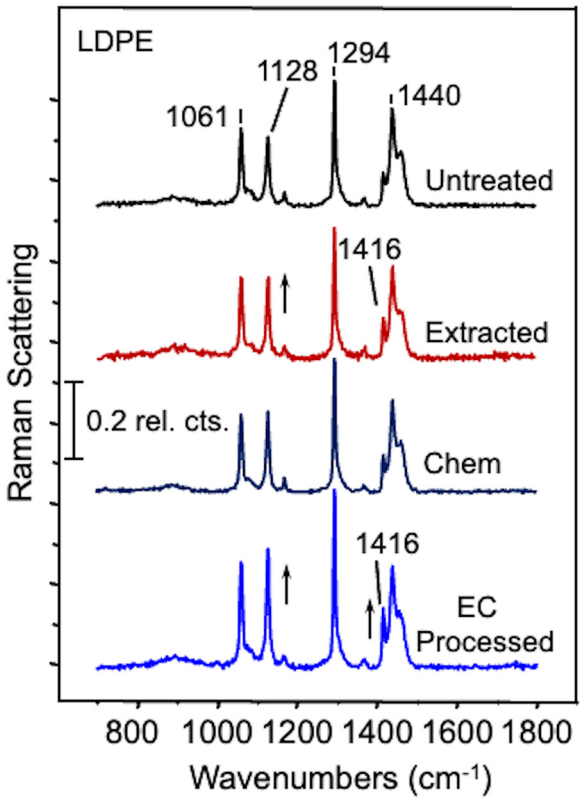

Figure 2. Raman spectra recorded from individual LDPE particles in contact with the surface of a glass microscope coverslip before (Untreated) and after hexane extraction (Extracted). The spectrum labeled "EC Processed" underwent electrochemical processing (in 1.0 M H_2SO_4 at Cu electrodes) following extraction in hexane.[8] The spectrum labeled "Chem" was subjected to the same chemical environment as the "EC Processed" sample, but the electrochemical potential program was not applied.

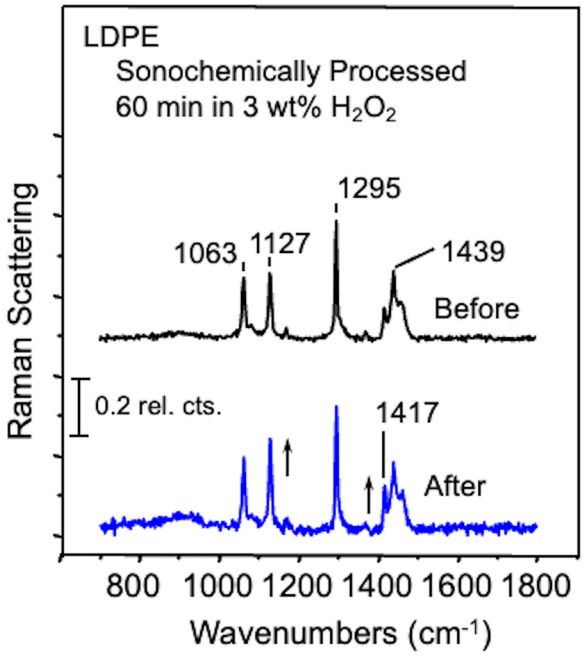

Figure 3. Raman spectra recorded from individual hexane-extracted LDPE particles prior to (before) and just following (after) sonication in 3 wt% H_2O_2 solution.

while viewing through the microscope eyepieces, care was taken to sample from positions where polymer/glass contact was evident.

While the spectra in Figure 2 display characteristic polyethylene features, slight differences in relative peak intensities among the samples indicate the influence of processing conditions on crystallinity within this near surface region.[39,41,42] Relative to the pristine (untreated) sample, growth in peaks near 1128 cm^{-1}, 1294 cm^{-1}, and 1418 cm^{-1} in spectra of the processed samples signals clear crystallinity enhancements resulting from the treatments.[38,39,41,42] The spectrum labeled "Extracted" in Figure 2 was recorded following hexane extraction of pristine particles to remove organic additives, mainly long chain alkane and fatty acid compounds.[8] Dispelling these relatively small molecules from the polymer matrix increases interactions between polyethylene chains, enabling neighboring trans chains to organize into ordered crystalline regions.[41,42] The spectrum labeled "EC Processed" in Figure 2 was recorded from particles that had undergone electrochemical processing[8] following extraction in hexane. Relative to the "Extracted" particles, the spectrum indicates further crystallinity increases have occurred resulting from the electrochemical treatment. The spectrum labeled "Chem" was subjected to the same steps as the "EC Processed" sample, except the electrochemical potential program was not applied. Instead, the cell stood at the open circuit potential for the duration of the reaction period. The spectral features of this "Chem" sample are not changed appreciably from those of the "Extracted" sample and indicate the structural differences evident in the spectrum labeled "EC Processed" are linked to the voltage program applied to the cell.

As a further test of the Raman microscopy characterization strategy, LDPE particles were analyzed following a procedure that used sonochemistry to assist material decomposition.[43,44] After suspension in dilute (3 wt%) hydrogen peroxide, the solution was sonicated for 60 minutes to accelerate the formation of hydroxyl radicals[43–48] and related reactive oxygen species[49] that promote oxidative decomposition reactions at the surface and near-surface regions of the particles. Raman spectra recorded from individual hexane extracted LDPE particles prior to and just following sonication are shown in Figure 3. The growth in peaks near 1127 cm^{-1} and 1417 cm^{-1} is clear evidence for crystallinity change in connection with the sonochemically assisted processing steps. In contrast, LDPE particles suspended in ultrapure water and sonicated for 60 minutes or suspended in 3 wt% H_2O_2 without sonication showed little evidence of degradation.

Depth-Profiling Within Individual Particles. Taking advantage of the spatial resolution capabilities of the Raman microscope system (< 2 μm, vide infra), the ability to measure chemical composition at different depths within an individual particle was explored. The spectra in Figure 4 reflect changes in LDPE crystallinity within individual particles as the confocal probe volume was moved from the surface (indicated as 0 μm) to positions deeper inside the particle. The left panel shows typical results obtained for pristine LDPE. The peak energies and relative intensities of the bands across the spectral dataset appear constant, indicating the sample composition within the region ~20 μm from the surface is quite uniform. In contrast, the middle panel of Figure 4 displaying a set of spectra that probe within a particle of hexane-extracted LDPE reveal notably strong crystallinity changes at the particle surface and diminishing crystallinity enhancement with increasing probe depth. The structural phase composition gradient that develops likely reflects a greater ease of extracting low molecular weight additives from the surface region of pristine LDPE particles than from the bulk material. In general, compared to the pristine LDPE sample, the hexane-extracted particles showed much greater structural heterogeneity on the micrometer length scale probed by the Raman measurements. The tendency for some regions within a hexane-extracted particle to become especially rich in the crystalline phase, while other regions retain greater amorphous character, likely results from limited polymer chain mobility creating barriers to additive removal and subsequent crystalline phase development.

The panel at the right in Figure 4 displays spectra recorded from hexane-extracted LDPE after the sample was further processed by sonication in dilute aqueous H_2O_2 solution. The spectral series shows evidence for crystallinity enhancement in the near surface region and persistence of the enhancement to a distance of at least 40 μm further into the particle. Depth-profiling of LDPE samples was limited to about 40 μm, as signal decline traceable to the depth-dependent loss in the efficiency of collecting Raman backscattered radiation from within polymers[9,16,17] occurred beyond this point. The lower collection efficiency is reflected in the noise at the baseline in the 35 μm and 40 μm position spectra in Figure 4. Normalizing spectra to the intensity of the strong anti-symmetric CH_2 stretching band near 2882 cm^{-1} enables comparisons among spectra by putting peaks on a common scale relative to the strongest in the spectrum and highlights the spectral signal-to-noise ratio decline when the overall Raman scattering intensities become low.

The instrument depth resolution was estimated by scanning the confocal probe volume through single layer graphene sheet[13,14] and model polymer–polymer[10,11,13] interfaces. The response recorded from single layer graphene, plotting the intensity of the graphene 2D vibrational band as a function of axial (z-direction) position as the confocal probe volume translates through the sample (Figure S1, Supplemental

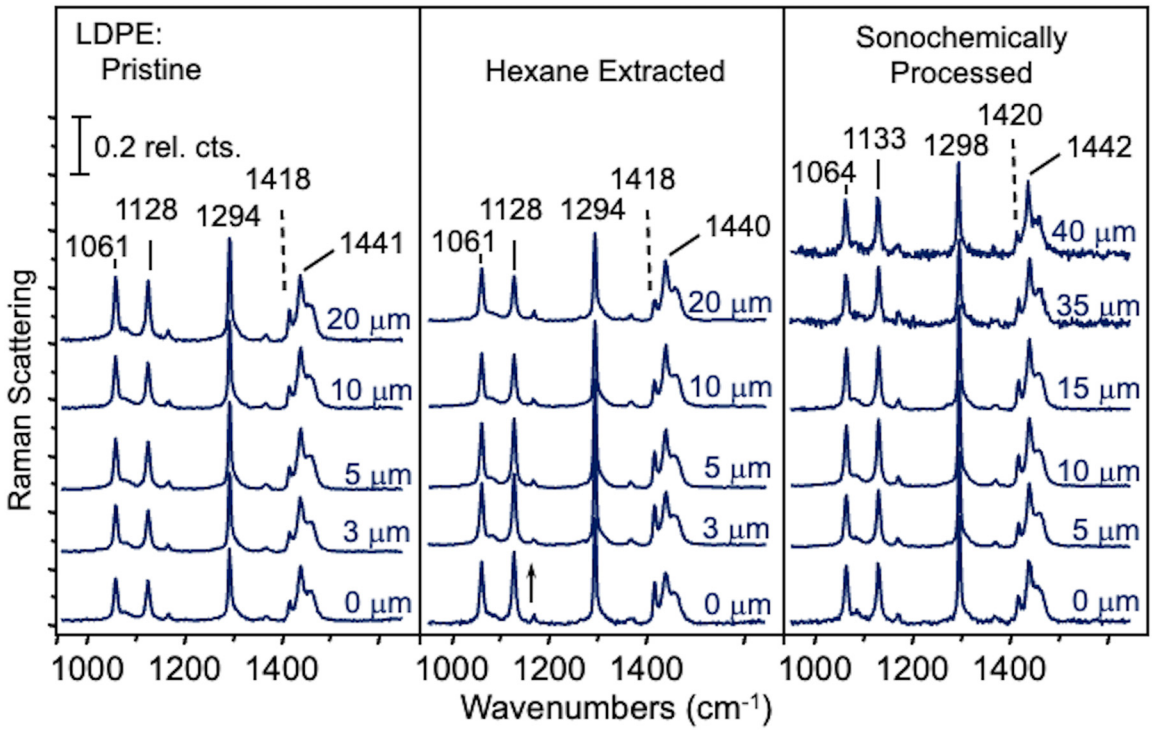

Figure 4. Raman spectra recorded as a function of depth below the surface of an individual LDPE particle prior to any processing (left panel) and following hexane extraction (center panel) and subsequent sonication in 3 wt% H_2O_2 solution (right panel).

Material), traces the detection efficiency profile for the instrument.[10,11,13,14] When fit to a Lorentzian line shape function, the full width half-maximum (FWHM) parameter provides an estimate of the axial spatial resolution.[9–13,50] For measurements performed on the graphene sheet, the FWHM value of 1.3 μm is consistent with earlier determined values for Raman instruments equipped with a high NA oil-immersion objective.[10,11,13] The breadth (1.3 μm) reflects the optical aberrations that decrease axial spatial resolution relative to the ideal diffraction limited response for the objective and confocal system used (0.4 μm).[9,12,13,26]

The FWHM derived from the Lorentzian fit in Figure S1 is a measure of the probe volume depth along the z-direction encompassing the region of 50% detection efficiency.[9–13] Recently, Sacco and co-workers advocated fitting confocal Raman depth profiles of SLG to a Gaussian line shape function and defining the 95.5% detection efficiency as $1.699 \times \mathrm{FWHM} = 4\sigma$, in which σ is the Gaussian width parameter.[14] Using the latter approach, the FWHM derived from the Gaussian fit of data in Figure S1 is 1.5 μm and predicts a 95.5% detection efficiency of ±1.3 μm (or $4\sigma = 2.6$ μm). These spatial resolution capabilities were confirmed in depth profiles recorded from a sharp boundary separating a model polymer–polymer interface (Figure S2, Supplemental Material). In this case, the profile of each phase was well fit by calculating the convolution of a step function representing the ideal material phase boundary with a Lorentzian line shape function representing the instrument detection efficiency profile.[10–13] The profile FWHM parameter derived from the analysis (1.5 μm) is close to the value of 1.3 μm measured using SLG (Figure S1).

To examine the extent to which these spatial resolution estimates apply in measurements within the near surface region of the micrometer-scale polymer particles of interest, depth profiles were recorded from a polymer–polymer interface formed by a spherical polystyrene particle imbedded within a PDMS matrix (Figure 5). The materials were selected based on their distinguishing vibrational bands at 1001 cm^{-1} (polystyrene) and 490 cm^{-1} (PDMS), as depicted in Figure 5b. The spherical polystyrene particles were shown in earlier studies to be useful standards for confocal Raman microscopy depth profiling.[12] Both the spheres[12] and PDMS[13] employed have sufficient transparency to support measurements at the limited depths required for the experiment (< 30 μm). The depth profile in Figure 5a was constructed by plotting the intensities of the two bands as a function of position starting with the probe about 3 μm above the coverslip. The polystyrene signal reaches a maximum as the confocal probe volume progresses upward through the central region of the 10 μm particle and begins a steep decline in crossing the polystyrene–PDMS interface. As in Figure S2, the solid lines on the plot show the response for a Lorentzian instrument detection efficiency profile convoluted with a step function representing the interface between polymer phases.[10–13] The analysis neglects the interface curvature and ability of the spherical particles to focus forward scattered radiation that back reflects toward the objective from the polystyrene–PDMS interface.[12] The latter effect can contribute to the slight arc in the measured responses over the 3–10 μm range in Figure 5a as the confocal probe volume translates through the particle. The spatial resolution suggested by the profiles in Figure 5a (~2 μm) is in good agreement with the limiting resolution measured using SLG and sufficient to detect composition changes occurring over the range of 20 μm–40 μm examined in Figure 4.

Figure S3 (Supplemental Material) shows the strong modifying effect electrochemical processing can have on the surface of LDPE particles. Sampling at the 20 μm depth, spectra

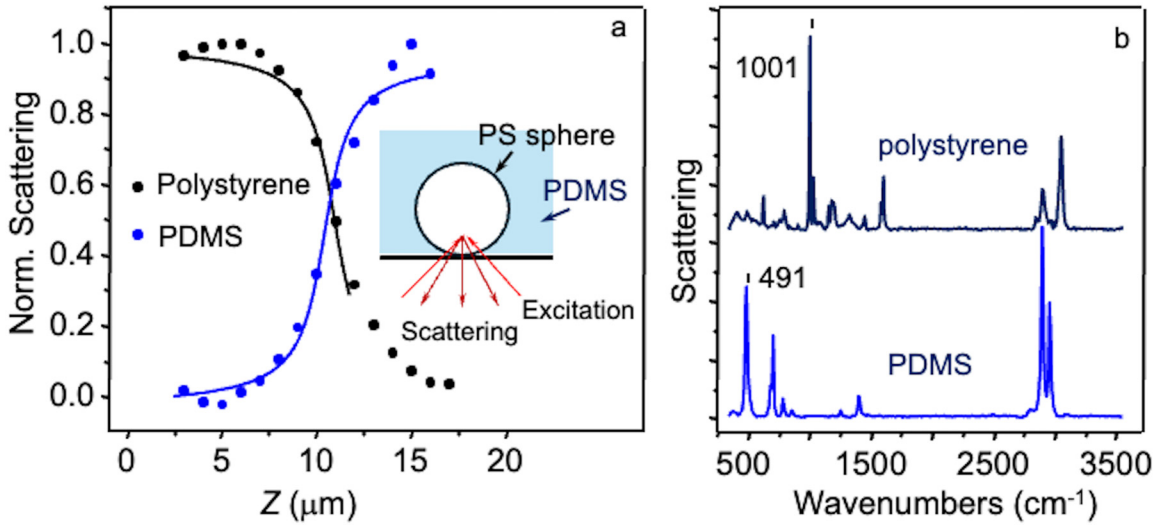

Figure 5. Raman spectra recorded as a function of depth below the surface of a model polymer–polymer interface constructed by imbedding a spherical polystyrene particle within a PDMS matrix.

display crystallinity enhancement comparable to that observed for particles after sonication in dilute aqueous H_2O_2 solution (Figure 4, left panel). However, much stronger crystallinity enhancement is evident when probing a few micrometers from the surface (Figure S3, bottom). The finding has motivated further studies aimed at improving the electrochemical processing technique and understanding interactions of polymer within the electrode–solution interfacial region.

It is important to note that the spatial resolution attained in the reported depth-profiling work depends critically on the properties of the microscope objective.[9,10,12,13] Objectives designed to focus into the sample through an air gap, like those often available for confocal Raman microscopy, suffer when probing beneath a polymer surface due to deleterious effects of refraction stemming from the relatively large air–sample refractive index difference.[9,10,17] Reducing this difference through use of an objective designed for use with an immersion fluid improves the ability to tightly focus excitation radiation within the sample and collect Raman scattered light from the region with high efficiency.[9,12,17] For example, based simply on the diffraction-limited spatial resolution, relative to a high collection efficiency air-objective (e.g., NA 0.9) the oil-immersion objective used in the reported work improves the spatial resolution by more than a factor of two ($1.4^2/0.9^2$).[9,14,17] Further, the refractive index matching achieved nearly eliminates the deleterious effects from depth-scale compression[9,10] and spherical aberration (e.g., depth dependent probe beam distortion) that, as Everall and others have pointed out,[9] can greatly complicate probing beneath the surface of materials with an air-objective.[9,10,17] Thus, use of an oil-immersion objective in the reported studies minimized optical distortions and provided good accuracy in depth-profiling the near surface region of the polymer materials investigated.[9,10,12,13]

Repeated Sampling of Particles. As a step toward assessing variability in material structure and composition at different positions within a particle and among particles that make up a sample, results of repeated sampling were analyzed. For pristine polyethylene, the approach revealed uniformity consistent with the depth-profiling results in Figure 4. Measuring at a constant depth of 20 μm, a dataset composed of 20 Raman spectra collected from different particles and sites within each particle was decomposed using PCA, following an approach used by Sato and coworkers[38] to predict polyethylene density from Raman spectra. Figure S4 (bottom set) displays the first two spectral vectors (PCA loadings) returned from the analysis. The first, labeled v1, reflects the average response across the dataset and is closely similar to the LDPE spectrum in Figure 1. The calculated Hotelling's T-squared statistic indicates this first loading accounts for > 99.9% of the variance in the dataset. The second, labeled v2, consists mainly of random noise and is similar to the remaining loadings (v3–v20). With only one significant loading (v1), the PCA results indicate the pristine polyethylene particles have a consistent composition and structure with little variation from particle-to-particle and at different sites within the near surface region of individual particles. Results of similar measurements performed on hexane extracted particles and samples before and after processing steps are included in the Figures S4–S5 (Supplemental Material).

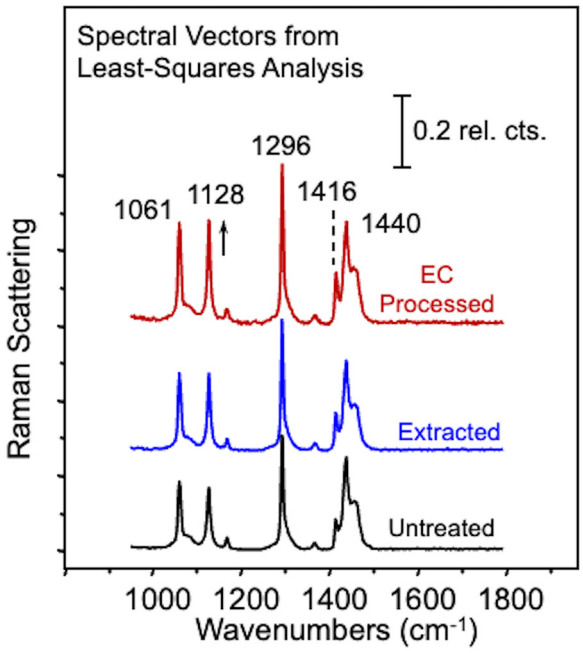

Figure 6. Pure component spectra of pristine (Untreated), hexane-extracted (Extracted) and electrochemically processed (EC Processed) LDPE derived from least-squares modeling of Raman spectral datasets.

Although PCA provides a convenient approach for scrutinizing large datasets, since the widespread availability of computers makes decomposition of the variance–covariance matrix to an orthogonal basis rapid and simple, the spectral vectors derived are complicated, with peaks that can extend in both upward and downward directions,[33,34] as Figures S4–S5 depict. It is possible to obtain more physically meaningful spectral vectors that can be related to the chemically pure components of a sample by performing least-squares modeling of the data matrix.[33,35–37] Example results obtained from datasets derived from Raman spectra of processed LDPE samples are shown in Figure 6.

The approach decomposes a matrix of spectral data (**D**) into a matrix of pure-component spectra (**A**) and a coefficient (or concentration) matrix (**C**) according to the following equation: $\mathbf{D} = \mathbf{A} \times \mathbf{C}$.[33,35–37] When the spectra in **D** are in columns, the pure-component spectra in **A** are also in columns and the elements of **C** ($c(i,j)$) specify the fractional contribution of each pure component (i) to each measured spectrum (j). These **A** and **C** matrices can be related to

the PCA scores and loadings for the dataset through a linear transformation, as elaborated in Section S.2 (Supplemental Material).

The spectral vectors in Figures 6 were derived assuming the experimental spectra are composed of two components, one reflecting the bulk polymer and the second dominated by effects of processing. The values of the Hotelling's T-squared statistic returned in the factor analysis (98.89, 1.02, and 0.03 for the first, second and third principal component, respectively, from spectra of electrochemically processed samples (see above for the values from the analysis of hexane extracted samples) support this assumption, as they show the great majority of variation in the dataset is contained within two spectral (loading) vectors.[33] Thus, **A** was constrained to have two columns and **C** two rows.

The responses in Figure 6 labeled "Untreated" and "Extracted" are the two pure component spectra obtained from least-squares modeling of the dataset from which the loading vectors in Figure S4 (upper) were derived. Following the iterative procedure,[35–37] the coefficients in **C** were optimized starting from an initial pair of spectra in **A** drawn at random, one from each group (untreated versus hexane extracted) in the dataset. The optimization was subject to a simple model that applied constraints to the coefficients in **C**. Specifically, for each spectrum, *j*, the corresponding concentration coefficients ($c(1,j)$ and $c(2,j)$), were required to be positive and sum to 1.0, reflecting the relationship of the coefficients to the mole fraction of each pure component present within the spatial region of a particle from which spectra were recorded.[33,35–37] As anticipated, of the two pure component spectra in Figure 6, one (labeled Untreated) displays characteristics of bulk LDPE and the other (labeled Extracted) shows features of the crystallinity enriched material that develops with processing. These optimized pure component vectors were found independent of the spectra selected for initialization of **A**, even when both were from samples before or after processing. Most notable–compared to the PCA derived spectral vectors (Figure S4, upper), those obtained from least-squares modeling with experimentally meaningful constraints applied in the optimization of the concentration coefficients display normal upward-extending features that can be understood in terms of the chemical composition of the sample.

The top spectrum in Figure 6 (labeled "EC Processed") was obtained from least-squares modeling of the dataset from which the loadings in Figure S5 (upper) were decomposed. One of the two resultant pure component spectra, it reflects material changes associated with electrochemical processing. The second pure component vector (plotted in Figure S6) is dominant in spectra of hexane extracted LDPE particles and is nearly identical to the related pure component spectrum in Figure 6 (middle). Again, the least squares derived pure component spectra (Figure 6, top, and Figure S6) appear as normal Raman spectra without complication from derivative-shaped bands, in contrast to the loading vectors obtained from PCA decomposition (Figure S5, Supplemental Material). The quality of the least squares derived model is depicted in Figure S7, which plots an original spectrum for each sample along with its residual. The residuals are generally at the noise level of the original spectra with little remaining structure. The plots in Figure S7 are representative of responses across the dataset. In reference to Figure 6, progressing from the pristine (Untreated) to the hexane-extracted (Extracted) and then the electrochemically processed (EC Processed) sample shows the expected growth in the crystallinity sensitive bands near 1128 cm^{-1} and 1418 cm^{-1} and demonstrates a useful application of least-squares modeling combined with Raman microscopy as an aid to assessing the effectiveness of processing conditions on material properties.

Conclusion

Confocal Raman microscopy performed with a high NA oil-immersion objective can be easily applied for high spatial resolution (< 2 μm) depth-profiling of compositional and structural change within the near-surface region of individual, micrometer-scale polymer particles subjected to chemical processing. The sampling configuration promotes refractive index matching, helping to overcome limitations of the air-objectives equipped on typical confocal Raman microscopes. For the polyethylene materials studied, vibrational bands sensitive to crystallinity and conformational order[38,39,41,42] were effective indicators of material transformations following chemical and electrochemical[8] treatments. In depth profiling to a distance 40 μm from the polymer surface, the composition of the pristine material showed remarkable uniformity. In contrast, processed particles displayed an enhancement in surface crystallinity and changes in material crystallinity with increasing depth that reflect the effectiveness of treatments toward polymer deconstruction. Toward measurements on ensembles of particles, PCA and least-squares modeling are useful for discerning processing-induced changes, with the latter providing pure component spectra that reflect crystallinity change within spectral datasets. The studies demonstrate an approach for monitoring reaction progress as strategies for polymer recycling and upcycling are advanced.

Acknowledgments

We gratefully acknowledge financial support from the U.S. Department of Energy (DOE) Office of Basic Energy Sciences (G. G.B.) and the U.S. National Science Foundation (NSF, C.K.) through grants DE-SC0022307 (DOE) and CBET-1922956 (NSF) and thank Mr. Rasoul Rahimzadeh for preparing the electrochemically processed samples analyzed. CK is thankful to helpful discussions with Jay P. Kitt (U Utah) and Joel M. Harris (U Utah) over the years concerning confocal Raman microscopy measurements and statistical treatments of spectral data.

ORCID iDs

Md. Wahiduzzaman https://orcid.org/0009-0007-5592-551X
Jeremy Lawrence https://orcid.org/0000-0001-7188-0728
Gerardine G. Botte https://orcid.org/0000-0002-5678-6669
Carol Korzeniewski https://orcid.org/0000-0003-3672-0731

Supplemental Material

All supplemental material mentioned in the text is available in the online version of the journal.

References

1. R. Geyer, J.R. Jambeck, K.L. Law. "Production, Use, and Fate of All Plastics Ever Made". Sci. Adv. 2017. 3(7): e1700782. 10.1126/sciadv.1700782
2. S.B. Borrelle, J. Ringma, K.L. Law, C.C. Monnahan, et al. "Predicted Growth in Plastic Waste Exceeds Efforts to Mitigate Plastic Pollution". Science. 2020. 369(6510): 1515–1581. 10.1126/science.aba3656
3. D. Elkhatib, V. Oyanedel-Craver. "A Critical Review of Extraction and Identification Methods of Microplastics in Wastewater and Drinking Water". Environ. Sci. Technol. 2020. 54(12): 7037–7049. 10.1021/acs.est.9b06672
4. C. Schwaferts, V. Sogne, R. Welz, F. Meier, et al. "Nanoplastic Analysis by Online Coupling of Raman Microscopy and Field-Flow Fractionation Enabled by Optical Tweezers". Anal. Chem. 2020. 92(8): 5813–5820. 10.1021/acs.analchem.9b05336
5. R. Gillibert, G. Balakrishnan, Q. Deshoules, M. Tardivel, et al. "Raman Tweezers for Small Microplastics and Nanoplastics Identification in Seawater". Environ. Sci. Technol. 2019. 53 (15): 9003–9013. 10.1021/acs.est.9b03105
6. S.L. Wright, J.M. Levermore, F.J. Kelly. "Raman Spectral Imaging for the Detection of Inhalable Microplastics in Ambient Particulate Matter Samples". Environ. Sci. Technol. 2019. 53 (15): 8947–8956. 10.1021/acs.est.8b06663
7. J.M. Levermore, T.E.L. Smith, F.J. Kelly, S.L. Wright. "Detection of Microplastics in Ambient Particulate Matter Using Raman Spectral Imaging and Chemometric Analysis". Anal. Chem. 2020. 92(13): 8732–8740. 10.1021/acs.analchem.9b05445
8. R. Rahimzadeh, J. Ortega-Ramos, Z. Haque, G.G. Botte. "Electrochemical Oxidation and Functionalization of Low-Density Polyethylene". ChemElectroChem. 2023. 10(10): e202300021. 10.1002/celc.202300021
9. N.J. Everall. "Confocal Raman Microscopy: Common Errors and Artefacts". Analyst. 2010. 135(10): 2512–2522. 10.1039/c0an00371a
10. C.A. Froud, I.P. Hayward, J. Laven. "Advances in the Raman Depth Profiling of Polymer Laminates". Appl. Spectrosc. 2003. 57(12): 1468–1474. 10.1366/000370203322640099
11. C.J. de Grauw, N.M. Sijtsema, C. Otto, J. Greve. "Axial Resolution of Confocal Raman Microscopes: Gaussian Beam Theory and Practice". J. Microscopy. 1997. 188(3): 273–279. 10.1046/j.1365-2818.1997.2620818.x
12. T. Bridges, M. Houlne, J.M. Harris. "Spatially Resolved Analysis of Small Particles by Confocal Raman Microscopy: Depth Profiling and Optical Trapping". Anal. Chem. 2004. 76(3): 576–584. 10.1021/ac034969s
13. C. Korzeniewski, J.P. Kitt, S. Bukola, S.E. Creager, et al. "Single Layer Graphene for Estimation of Axial Spatial Resolution in Confocal Raman Microscopy Depth Profiling". Anal. Chem. 2019. 91(1): 1049–1055. 10.1021/acs.analchem.8b04390
14. A. Sacco, C. Portesi, A.M. Giovannozzi, A.M. Rossi. "Graphene Edge Method for Three-Dimensional Probing of Raman Microscopes Focal Volumes". J. Raman Spectrosc. 2021. 52 (10): 1671–1684. 10.1002/jrs.6187
15. S.-C. Huang, J.-Z. Ye, X.-R. Shen, Q.-Q. Zhao, et al. "Electrochemical Tip-Enhanced Raman Spectroscopy with Improved Sensitivity Enabled by a Water Immersion Objective". Anal. Chem. 2019. 91(17): 11092–11097. 10.1021/acs.analchem.9b01701
16. Z. Peng, P. Huguet, S. Deabate, A. Morin, A.K. Sutor. "Depth-Resolved Micro-Raman Spectroscopy of Tri-Layer PFSA Membrane for PEM Fuel Cells: How to Obtain Reliable Inner Water Contents". J. Raman Spectrosc. 2013. 44(2): 321–328. 10.1002/jrs.4192
17. S. Deabate, P. Huguet, A. Morin, G. Gebel, et al. "Raman Microspectroscopy as a Useful Tool for In Situ and Operando Studies of Water Transport in Perfluorosulfonic Membranes for PEMFCs". Fuel Cells. 2014. 14(5): 677–693. 10.1002/fuce.201300236
18. S. Bukola, K. Beard, C. Korzeniewski, J.M. Harris, S.E. Creager. "Single-Layer Graphene Sandwiched Between Proton-Exchange Membranes for Selective Proton Transmission". ACS Appl. Nano Mater. 2019. 2(2): 964–974. 10.1021/acsanm.8b02270
19. S. Bukola, Y. Liang, C. Korzeniewski, J. Harris, S.E. Creager. "Selective Proton/Deuteron Transport Through Nafion|Graphene|Nafion Sandwich Structures at High Current Density". J. Am. Chem. Soc. 2018. 140(5): 1743–1752. 10.1021/jacs.7b10853
20. T.E. Bridges, R.H. Uibel, J.M. Harris. "Measuring Diffusion of Molecules into Individual Polymer Particles by Confocal Raman Microscopy". Anal. Chem. 2006. 78(7): 2121–2129. 10.1021/ac052056n
21. J.P. Kitt, J.M. Harris. "Confocal Raman Microscopy for in Situ Measurement of Octanol-Water Partitioning Within Pores of Individual C18-Functionalized Chromatographic Particles". Anal. Chem. 2015. 87(10): 5340–5347. 10.1021/acs.analchem.5b00634
22. D.A. Bryce, J.P. Kitt, J.M. Harris. "Confocal Raman Microscopy for Label-Free Detection of Protein–Ligand Binding at Nanopore-Supported Phospholipid Bilayers". Anal. Chem. 2018. 90(19): 11509–11516. 10.1021/acs.analchem.8b02791
23. G.J. Myres, E.M. Peterson, J.M. Harris. "Confocal Raman Microscopy Enables Label-Free, Quantitative, and Structurally Informative Detection of DNA Hybridization at Porous Silica Surfaces". Anal. Chem. 2021. 93(22): 7978–7986. 10.1021/acs.analchem.1c00885
24. G.J. Myres, J.P. Kitt, J.M. Harris. "Inter-Leaflet Phospholipid Exchange Impacts the Ligand Density Available for Protein Binding at Supported Lipid Bilayers". Langmuir. 2022. 38(22): 6967–6976. 10.1021/acs.langmuir.2c00526
25. H.J. Harbin, D.K. Unruh, D.J. Casadonte, S.J. Khatib. "Sonochemically Prepared Ni-Based Perovskites as Active and Stable Catalysts for Production of Cox-Free Hydrogen and Structured Carbon". ACS Catal. 2023. 13(7): 4205–4220. 10.1021/acscatal.2c05672

26. J. Xu, M. Koh, S.D. Minteer, C. Korzeniewski. "In Situ Confocal Raman Microscopy of Redox Polymer Films on Bulk Electrode Supports". ACS Meas. Sci. Au. 2023. 3(2): 127–133. 10.1021/acsmeasuresciau.2c00064
27. J.P. Kitt, D.A. Bryce, J.M. Harris. "Spatial Filtering of a Diode Laser Beam for Confocal Raman Microscopy". Appl. Spectrosc. 2015. 69(4): 513–517. 10.1366/14-07671
28. K.P.J. Williams, G.D. Pitt, D.N. Batchelder, B.J. Kip. "Confocal Raman Microspectroscopy Using a Stigmatic Spectrograph and CCD Detector". Appl. Spectrosc. 1994. 48(2): 232–235. 10.1366/0003702944028407
29. Y. Wang, R.L. McCreery. "Evaluation of a Diode Laser/Charge Coupled Device Spectrometer for Near-Infrared Raman Spectroscopy". Anal. Chem. 1989. 61(23): 2647–2651. 10.1021/ac00198a012
30. M.A. Fryling, C.J. Frank, R.L. McCreery. "Intensity Calibration and Sensitivity Comparisons for CCD/Raman Spectrometers". Appl. Spectrosc. 1993. 47(12): 1965–1974. 10.1366/0003702934066226
31. S.J. Choquette, E.S. Etz, W.S. Hurst, D.H. Blackburn, S.D. Leigh. "Relative Intensity Correction of Raman Spectrometers: NIST SRMs 2241 Through 2243 for 785 nm, 532 nm, and 488 nm/514.5 nm Excitation". Appl. Spectrosc. 2007. 61(2): 117–129. 10.1366/000370207779947585
32. N.N. Brandt, O.O. Orovko, A.Y. Chikishev, O.D. Paraschuk. "Optimization of the Rolling-Circle Filter for Raman Background Subtraction". Appl. Spectrosc. 2006. 60(3): 288–293. 10.1366/000370206776342553
33. E.R. Malinowski. Factor Analysis in Chemistry. New York: Wiley, 2002.
34. J.R. Beattie, F.W.L. Esmonde-White. "Exploration of Principal Component Analysis: Deriving Principal Component Analysis Visually Using Spectra". Appl. Spectrosc. 2021. 75(4): 361–375. 10.1177/0003702820987847
35. D. Rivera, P.E. Peterson, R.H. Uibel, J.M. Harris. "In Situ Adsorption Studies at Silica/Solution Interfaces by Attenuated Total Internal Reflection Fourier Transform Infrared Spectroscopy: Examination of Adsorption Models in Normal-Phase Liquid Chromatography". Anal. Chem. 2000. 72(7): 1543–1554. 10.1021/ac990968h
36. C. Korzeniewski, E. Adams, D. Liu. "Responses of Hydrophobic and Hydrophilic Groups in Nafion Differentiated by Least Squares Modeling of Infrared Spectra Recorded During Thin Film Hydration". Appl. Spectrosc. 2008. 62(6): 634–639. 10.1366/000370208784658075
37. C. Korzeniewski, E.M. Peterson, J.P. Kitt, S.D. Minteer, J. M. Harris. "Adapting Confocal Raman Microscopy for in Situ Studies of Redox Transformations at Electrode–Electrolyte Interfaces". J. Electroanal. Chem. 2021. 896: 115207. 10.1016/j.jelechem.2021.115207
38. H. Sato, M. Shimoyama, T. Kamiya, T. Amari, et al. "Raman Spectra of High-Density, Low-Density, and Linear Low-Density Polyethylene Pellets and Prediction of Their Physical Properties by Multivariate Data Analysis". J. Appl. Polym. Sci. 2002. 86(2): 443–448. 10.1002/app.10999
39. D. Oldak, H. Kaczmarek, T. Buffeteau, C. Sourisseau. "Photo- and Bio-Degradation Processes in Polyethylene, Cellulose and Their Blends Studied by ATR-FTIR and Raman Spectroscopies". J. Mater. Sci. 2005. 40: 4189–4198. 10.1007/s10853-005-2821-y
40. R.G. Snyder, S.L. Hsu, S. Krimm. "Vibrational Spectra in the C–H Stretching Region and the Structure of the Polymethylene Chain". Spectrochim. Acta. 1978. 34(4): 395–406. 10.1016/0584-8539(78)80167-6
41. Y. Hiejima, T. Kida, K. Takeda, T. Igarashi, K. Nitta. "Microscopic Structural Changes During Photodegradaation of Low-Density Polyethylene Detected by Raman Spectroscopy". Polym. Degrad. Stab. 2018. 150: 67–72. 10.1016/j.polymdegradstab.2018.02.010
42. B.R. Kang, S.B. Kim, H.A. Song, T.K. Lee. "Accelerating the Biodegradation of High-Density Polyethylene (HDPE) Using *Bjerkandera adusta* TBB-03 and Lignocellulose Substrates". Microorganisms. 2019. 7(9): 304. 10.3390/microorganisms7090304
43. G.J. Price. "Polymer Sonochemistry: Controlling the Structure and Properties of Macromolecules". In: L.A. Crum, T.J. Mason, J.L. Reisse, K.S. Suslick, editors. Sonochemistry and Sonoluminescence. Dordrecht, Netherlands: Kluwer Academic Publishers, 1999. Pp. 321–343. 10.1007/978-94-015-9215-4_25
44. D.J. Casadonte, J. McCoury, B. Korremula. "Heterodyne I: Enhancing Sonochemical Efficiency Through Application of the Heterodyne Effect: An Initial Study". Ultrason. Sonochem. 2019. 56: 143–149. 10.1016/j.ultsonch.2019.04.014
45. P. Riesz, T. Kondo. "Free Radical Formation Induced by Ultrasound and Its Biological Implications". Free Radic. Biol. Med. 1992. 13(3): 247–270. 10.1016/0891-5849(92)90021-8
46. C. Petrier, A. Jeunet, J.L. Luche, G. Reverdy. "Unexpected Frequency Effects on the Rate of Oxidative Processes Induced by Ultrasound". J. Am. Chem. Soc. 1992. 114(8): 3148–3150. 10.1021/ja00034a077
47. D.J. Casadonte Jr., M. Flores, C. Petrier. "The Use of Pulsed Ultrasound Technology to Improve Environmental Remediation: A Comparative Study". Environ. Tech. 2005. 26(12): 1411–1416. 10.1080/09593332608618615
48. D.J. Casadonte Jr., M. Flores, C. Petrier. "Enhancing Sonochemical Degradation of Environmental Contaminants Using Power-Modulated Pulsed Ultrasound: An Initial Study". Ultrason. Sonochem. 2005. 12(3): 147–152. 10.1016/j.ultsonch.2003.12.004
49. X. Xing, S. Zhao, T. Xu, L. Huang, et al. "Advances and Perspectives in Organic Sonosensitizers for Sonodynamic Therapy". Coord. Chem. Rev. 2021. 445: 214087. 10.1016/j.ccr.2021.214087
50. D.E. Koppel, D. Axelrod, J. Schlessinger, E.L. Elson, W.W. Webb. "Dynamics of Fluorescence Marker Concentration as a Probe of Mobility". Biophys. J. 1976. 16(11): 1315–1329. 10.1016/S0006-3495(76)85776-1